Bed load transport in turbulent flow at the grain scale: Experiments and modeling

E. Lajeunesse, L. Malverti, F. Charru

Bed load transport in turbulent flow at the grain scale: Experiments and modeling

E. Lajeunesse,[1] L. Malverti,[1] and F. Charru[2]

[1]   We report an experimental investigation of the motion of bed load particles under steady and spatially uniform turbulent flow above a flat sediment bed of uniform grain size. Using a high-speed video imaging system, we recorded the trajectories of the moving particles and measured their velocity and the length and duration of their flights, as well as the surface density of the moving particles. Our observations show that entrained particles exhibit intermittent motion composed of the succession of periods of "flight" and periods of rest. During one flight, a particle may go through phases of reptation, during which it moves in nearly persistent contact with the rough bed, and phases of saltation, during which it travels sufficiently high above the bed to reach high velocities. The distributions of longitudinal and transverse particle velocities obey a decreasing exponential and a Gaussian law, respectively. Interestingly, these observations are similar to those previously reported for viscous flows. The experimental results presented here support the erosion-deposition model of Charru (2006) and allow the calibration of the involved coefficients. In particular, noting τ^*, the Shields number, and τ_c^*, the threshold Shields number, we find that (1) the surface density of moving particles increases linearly with $\tau^* - \tau_c^*$; (2) the average particle velocity increases linearly with $\tau^{*1/2} - \tau_c^{*1/2}$, with a finite nonzero value at the threshold; (3) the flight duration scales with a characteristic settling time with no significant dependence on either τ^* or the settling Reynolds number; and (4) the flight length increases linearly with $\tau^{*1/2} - \tau_c^{*1/2}$. The results presented in this paper should provide a valuable physical framework to describe bed form development in turbulent flows.

Citation: Lajeunesse, E., L. Malverti, and F. Charru (2010), Bed load transport in turbulent flow at the grain scale: Experiments and modeling, *J. Geophys. Res.*, *115*, F04001, doi:10.1029/2009JF001628.

1.   Introduction

[2]   Bed load transport, which results from the motion of particles rolling, sliding or traveling in a succession of low jumps or "saltations" along the bed of a stream, is of fundamental importance for river morphodynamics. It may indeed represent an important fraction of the total sediment flux transported in a river (up to 60%), especially in gravel bed rivers [*Métivier et al.*, 2004; *Meunier et al.*, 2006; *Liu et al.*, 2008]. Many aspects of morphologic changes in rivers are governed by bed load transport, including bank erosion, bed forms and the rate at which the river incises relief [*Yalin*, 1977; *Dietrich and Smith*, 1984; *Gomez*, 1991; *Graf and Altinakar*, 1996; *Yalin and Ferreira da Silva*, 2001]. Despite the large number of works addressing the problem (and summarized hereafter), bed load transport remains poorly understood to this day with two important consequences for earth sciences: (1) landscape evolution models still rely on empirical laws with no physical basis [*Crave and Davy*, 2001; *Braun and Sambridge*, 1997; *Carretier and Lucazeau*, 2005]; (2) estimates of denudation rates from transport data often neglect the contribution of bed load or involve arbitrary assumptions about its importance [*Ahnert*, 1970; *Summerfield and Hulton*, 1994].

[3]   Most of the laws for bed load transport proposed in the literature consist of semiempirical equations derived from a fit of data acquired in flume experiments, with few consideration of the physics at the grain scale. Accordingly, our objective in this paper is to describe bed load transport at the grain scale. This was achieved by developing an experimental apparatus allowing the investigation of the motion of bed load particles under steady and spatially uniform turbulent flow above a flat sediment bed of uniform grain size. As discussed in the following, the originality of our approach with respect to previous investigations is that (1) our experiments are interpreted within the frame of an erosion-deposition model proposed by *Charru* [2006], thus determining the choice of the measured quantities, the measurement methods, and the way to analyze the data, and (2) contrarily to the majority of bed load transport laws proposed in the literature,

[1]Laboratoire de Dynamique des Fluides Geologiques, Institut de Physique du Globe de Paris, Paris, France.
[2]Institut de Mécanique des Fluides de Toulouse, CNRS/Université de Toulouse, Toulouse, France.

Table 1. Most Commonly Used Formulas to Describe Bed Load Transport in a Turbulent Flow[a]

Authors	Transport Rate q^*	Comments
Meyer-Peter and Müller [1948]	$8\,(\tau^* - \tau_c^*)^{\frac{3}{2}}$	Derived from a fit of experimental data.
Wong [2003]	$3.97\,(\tau^* - \tau_c^*)^{\frac{3}{2}}$	Derived from a fit of experimental data.
Einstein [1950]	$12f\,(\tau^* - \tau_c^*)^{\frac{3}{2}}$	Theoretical derivation; f is a fitting parameter.
Bagnold [1973]	$\frac{V}{\mu\sqrt{Rgd}}\,(\tau^* - \tau_c^*)$	Theoretical derivation; μ is a friction coefficient and V is the average particle velocity.
Ashida and Michiue [1973]	$17\,(\tau^* - \tau_c^*)\left(\sqrt{\tau^*} - \sqrt{\tau_c^*}\right)$	Theoretical derivation and fit of experimental data.
Fernandez-Luque and Van Beek [1976]	$5.7\,(\tau^* - \tau_c^*)^{\frac{3}{2}}$	Derived from a fit of experimental data.
Engelund and Fredsoe [1976]	$18.74\,(\tau^* - \tau_c^*)\left(\sqrt{\tau^*} - 0.7\sqrt{\tau_c^*}\right)$	Theoretical derivation.
Bridge and Dominic [1984]	$\frac{\alpha}{\mu}\,(\tau^* - \tau_c^*)\left(\sqrt{\tau^*} - \sqrt{\tau_c^*}\right)$	Theoretical derivation and fit of experimental data; μ is a friction coefficient and α is a fitting parameter.

[a]This list is not exhaustive and other transport formulas can be found in the work by *García* [2006].

the model of *Charru* [2006] accounts for a relaxation effect which strongly influences the development of bed forms.

[4] One way to formulate the problem of sediment transport in rivers and to identify the relevant controlling parameters is to proceed to dimensional analysis. The volumetric sediment transport rate per unit river width q_s is expected to depend on eight parameters involving three dimensions (length, time, mass): the fluid density ρ, the sediment density ρ_s, the kinematic viscosity of water ν, the gravitational acceleration g, the flow depth H, the bed slope S, the characteristic sediment diameter D (usually the median diameter of the sediment bed), and the shear velocity u^*, defined from the shear stress exerted by the fluid flow on the river bed by $\tau = \rho u^{*2}$. Dimensional analysis leads to the following relation for the dimensionless sediment transport rate

$$q^* = f\left(\tau^*, Re_s, R, S, \frac{H}{D}\right), \qquad (1)$$

where

$$q^* = \frac{q_s}{\sqrt{RgD^3}}, \qquad (2)$$

$$\tau^* = \frac{u^{*2}}{RgD}, \qquad (3)$$

$$Re_s = \frac{\sqrt{RgD^3}}{\nu}, \qquad (4)$$

$$R = \frac{\rho_s - \rho}{\rho}. \qquad (5)$$

[5] The Shields number τ^* is a dimensionless shear stress [*Shields*, 1936], and Re_s is a settling Reynolds number defined with the characteristic settling velocity $V_s = \sqrt{RgD}$. Note that the particle Reynolds number $Re_* = u^*D/\nu$ is related to the above numbers by $Re_* = Re_s\sqrt{\tau^*}$.

[6] Determining the function f which relates q^* to the set of parameters τ^*, Re_s, R, S and H/D has been the goal of a huge number of works either theoretical [*Duboys*, 1879; *Einstein*, 1950; *Bagnold*, 1956, 1973; *Ashida and Michiue*, 1973; *Engelund and Fredsoe*, 1976; *Bridge and Dominic*, 1984],

experimental [*Meyer-Peter and Müller*, 1948; *Fernandez-Luque and Van Beek*, 1976; *Wong*, 2003; *Recking et al.*, 2009] or based on the analysis of field data [*Bagnold*, 1980; *Gomez*, 1991]. Commonly cited bed load transport laws are listed in Table 1. Although no relationship has gained universal acceptance, some general features are accepted.

[7] 1. Most formulas involve a threshold value of the Shields number τ_c^* below which no sediment is transported, depending on Re_s and S [*Shields*, 1936; *Wiberg and Smith*, 1987; *Lamb et al.*, 2008].

[8] 2. They all predict the same dependence $q^* \propto \tau^{*3/2}$ sufficiently far from the threshold i.e., in the limit $\tau^* \gg \tau_c^*$.

[9] Two main groups can be distinguished. The first one predicts $q^* \propto (\tau^* - \tau_c^*)^{3/2}$ [*Meyer-Peter and Müller*, 1948; *Einstein*, 1950; *Fernandez-Luque and Van Beek*, 1976; *Wong*, 2003] whereas the second one proposes $q^* \propto (\tau^* - \tau_c^*)(\sqrt{\tau^*} - \sqrt{\tau_c^*})$ [*Ashida and Michiue*, 1973; *Engelund and Fredsoe*, 1976; *Bridge and Dominic*, 1984]. These laws provide similar predictions far from threshold but exhibit significant differences close to threshold.

[10] An alternative way to consider the problem of bed load transport is to consider that q_s can be written

$$q_s = \delta v\, n\, V, \qquad (6)$$

where n (dimensions $[L]^{-2}$) is the surface density of moving particles i.e., the number of moving particles per unit bed area, V is their averaged velocity, and δv is the volume of an individual particle. A better insight into the problem of bed load transport can be gained from the separate modeling of V and n, that is, the determination of their dependence on the parameters τ^*, Re_s, R, S and H/D.

[11] This approach has motivated several investigations of bed load transport at the grain scale. *Francis* [1973], *Abbott and Francis* [1977] and later *Hu* [1996] and *Lee and Hsu* [1994] investigated experimentally the trajectory of an isolated grain propelled by a water stream over a *nonerodible bed*. A second group of investigators studied the trajectories of bed load particles over an *erodible bed* [*Fernandez-Luque and Van Beek*, 1976; *Van Rijn*, 1984; *Nino and Garcia*, 1994; *Charru et al.*, 2004]. All these authors concluded that small saltation jumps are the main form of bed load motion and tried to characterize the variation with D and τ^* of the average saltation height h_s, saltation length L_s

Table 2. Saltation Length L_s, Saltation Height h_s, and Average Particle Velocity V Derived From Previous Experimental Investigations[a]

Authors	L_s	h_s	V	τ^*	S	Re_s	Re_*	H/D
Fernandez-Luque and Van Beek [1976]	$\frac{L_s}{D} = 16$		$V = 11.5\,(u^* - 0.7u_c^*)$	0.03–0.64	0.21–0.4	106–760	18–608	36–133
Abbott and Francis [1977]	dependency with τ^* no dependency with D	dependency with τ^* and D	$V = a\,(u^* - u_c^*)$, $a = 13.4$–14.3	0.0076–1.556	0–0.0184	717–3538	62–4413	3–14
Sekine and Kikkawa [1992]	$\frac{L_s}{D} = 3000 \cdot \tau^{*1/4}\left(\sqrt{\tau^*} - \sqrt{\tau_c^*}\right)$		$V = 8 \cdot (u^{*2} - u_c^{*2})^{1/2}$	0.043–0.233		120–3836	25–1852	
Nino and Garcia [1994]	$\frac{L_s}{D} = 2.3\,\frac{\tau^*}{\tau_c^*}$	dependency with τ^*/τ_c^* and D	$V = a\,(u^* - u_c^*)$, $a = 6.8$–8.5	0.09–0.14	0.03–0.07	7400–21,900	2220–8200	2.6–4.7
Lee and Hsu [1994]	$\frac{L_s}{D} = 196.3 \cdot (\tau^* - \tau_c^*)^{0.788}$	$\frac{h_s}{D} = 14.3(\tau^* - \tau_c^*)^{0.575}$	$V = 11.53\,u^*\,(\tau^* - \tau_c^*)^{0.174}$	0.06–0.5	0.002–0.023	200–493	50–75	20–90
Hu [1996]	$\frac{L_s}{D} = 27.5 \cdot \left(\frac{\rho_s}{\rho}\right)^{0.94} \tau^{*0.9}$	$\frac{h_s}{D} = 1.78\left(\frac{\rho_s}{\rho}\right)^{0.86} \tau^{*0.69}$	$V = 11.9\,(u^* - 0.44u_c^*)$	0.07–1.67	0.001–0.014	58–1018	15–1315	21–60

[a]Note that the equations of *Fernandez-Luque and Van Beek* [1976], *Abbott and Francis* [1977], *Sekine and Kikkawa* [1992], and *Nino and Garcia* [1994] rely on dimensional analysis whereas the formulas of *Lee and Hsu* [1994] and *Hu* [1996] result from a purely empirical fit of experimental data. The ranges of Shields numbers τ^*, bed slopes S, settling Reynolds numbers Re_s, particle Reynolds numbers Re_*, and H/D explored in these experiments are also indicated.

and particle velocity V. Their results are summarized in Table 2. Their conclusions about h_s and L_s are quite different. But, with the exception of *Lee and Hsu* [1994], they all found the same dependency for V
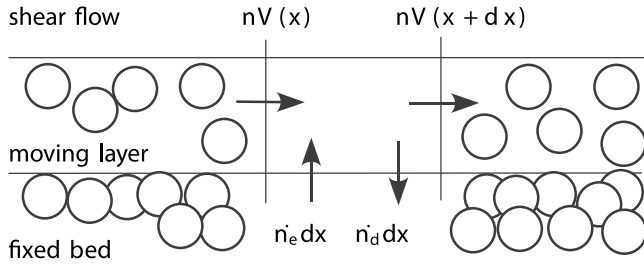
$$V = a(u^* - bu_c^*), \qquad (7)$$

where u_c^* is the threshold shear velocity, and a and b are positive coefficients related to the effective friction coefficient and an effective fluid velocity at the height of the grains. The values of a and b differ from one author to the other (see Table 2). V is positive so that $b \leqslant 1$. Note that the case $b = 1$ implies that the particle velocity cancels at the onset of sediment transport whereas $b < 1$ corresponds to a nonzero velocity $a(1 - b)u_c^*$ at threshold. Particle motion has also been investigated from numerical integration of the equation of motion of a particle, with simple models for the hydrodynamic forces. These lead to the same qualitative results [see e.g., *Wiberg and Smith*, 1989].

[12] All the bed load transport laws discussed so far establish a relation between the local flow rate of particles and the local shear stress exerted by the fluid flow on the bed. These relations consider implicitly that the particle flux is in equilibrium with the shear stress, so that their use in nonequilibrium conditions, i.e., when the shear stress varies in space or time, is questionable. Indeed, the particle flux does not respond instantaneously to a change of shear stress but adjusts itself with a spatial or temporal delay due to particle inertia or particle settling. This so-called relaxation effect is now recognized to have a strong influence on the development of bed forms, especially ripples [*Charru*, 2006]. In the case of sand particles in air flow, such relaxation effects have been introduced by *Sauermann et al.* [2001] and *Andreotti et al.* [2002] from a phenomenological first-order differential equation for the sand flux, which accounts for an inertial relaxation through an acceleration length $\ell_{acc} = \rho_s/\rho D$ of the grains. In water, whose density is much larger than that of air, *Charru* [2006] argued that this characteristic length would not be the most relevant one, and developed an erosion-deposition model of bed load transport for both viscous and turbulent flows. This model, which is described in section 2, was initially derived from viscous flow experiments [*Charru et al.*, 2004; *Charru and Hinch*, 2006], but has not been tested with turbulent flows. Indeed, despite the plethora of experimental investigations of bed load transport in a turbulent flow, measurements of relevant quantities such as V or n are either missing or inconsistent (see Table 2).

[13] In this paper, we investigate the motion of individual bed load particles entrained by a turbulent flow in a small experimental flume. Our objectives are to characterize the motion of individual bed load particles, to establish their relation to the macroscopic sediment transport and to analyze the measurements within the frame of the erosion-deposition model proposed by *Charru* [2006]. To this end, we performed systematic measurements of the velocity and surface density of the moving grains, together with the lengths and durations of the particle flights.

[14] The paper is organized as follows. In section 2, we briefly recall the derivation of the erosion-deposition model. Section 3 is dedicated to the description of the experimental setup and procedure. The experimental results are presented

Figure 1. Sketch of the particle fluxes in a strip of the moving layer, of length dx and width unity.

in section 4 and discussed in section 5. The paper ends with a summary of the results and conclusions.

2. Erosion-Deposition Model for Bed Load in a Turbulent Stream

[15] As stated by equation (6), the bed load flux is proportional to n, the surface density of moving particles. For steady and spatially uniform flow, this density corresponds to dynamical equilibrium between the particles eroded from the fixed bed and deposited onto it. For unsteady or non-uniform flow, such as that over ripples or dunes, this equilibrium may be broken, and the variation of $n(x, t)$ is governed by the conservation equation [*Charru and Hinch*, 2006]

$$\frac{\partial n}{\partial t} = \dot{n}_e - \dot{n}_d - \frac{\partial(nV)}{\partial x}. \tag{8}$$

This equation states that the variation rate of n is related to exchanges with the fixed bed, through the erosion rate $\dot{n}_e$ and the deposition rate $\dot{n}_d$ (both with dimension $[L]^{-2}[T]^{-1}$), and to the divergence of the bed load flux nV (Figure 1). To solve this equation, the mean particle velocity V and the erosion and deposition rates need to be modeled.

[16] The erosion and deposition rates can be determined from dimensional analysis as follows. As known from previous experiments and confirmed by the results presented in the following sections, particles within the moving layer have an intermittent behavior, composed of periods of motion, hereafter called "flights," with mean velocity V and characteristic duration t_d, alternating with periods of rest. During the deposition time t_d all particles stop once, so that the deposition rate can be written

$$\dot{n}_d = \frac{n}{t_d}. \tag{9}$$

The deposition time is controlled by gravity and expected to scale with the settling time D/V_s where V_s is the settling velocity. Thus, t_d can be written as

$$\frac{1}{t_d} = c_d \frac{V_s}{D}, \tag{10}$$

where c_d is a deposition coefficient to be determined from experiments.

[17] Erosion of a particle, which occupies the typical area D^2, occurs on a typical hydrodynamic timescale t_e, and can be written as

$$\dot{n}_e = \frac{1}{D^2 t_e}. \tag{11}$$

The erosion time t_e can be thought as that needed for a particle, submitted to the force $(\tau - \tau_c)D^2$, to escape the small trough or potential well where it is trapped, and reach some "escape velocity" which we take, for the sake of simplicity, to be the settling velocity V_s. Then, the time t_e can be defined from the inertial balance

$$\rho_s D^3 \frac{V_s}{t_e} = c_e (\tau - \tau_c)D^2, \tag{12}$$

where c_e is an erosion coefficient to be determined from experiments, as c_d. Note that another possible choice for t_e would be $D/(u^* - u_c^*)$, which is a timescale of the flow at the scale of the particle. However, as discussed below, this choice leads to a wrong prediction for n.

[18] Finally, the particle velocity can be modeled as proposed by *Bagnold* [1973], from a balance between the hydrodynamic force on a particle and a Coulomb friction force, leading to equation (7). The latter can be rewritten in terms of the Shields number,

$$\frac{V - V_c}{\sqrt{RgD}} = a\left(\sqrt{\tau^*} - \sqrt{\tau_c^*}\right), \tag{13}$$

where V_c, the particle velocity at the threshold of bed load transport, and the coefficient a have to be determined from experiments.

2.1. Steady and Uniform Flow Above a Flat Topography: The Saturated Regime

[19] Let us now consider two situations of particular interest. The first one is that of a steady and spatially uniform flow above a flat topography, where the erosion and deposition rates balance each other. Then, from (9) and (11), together with (10) and (12), the equilibrium or saturated density of moving particles is found to be

$$n_{sat}D^2 = \frac{t_d}{t_e} = \frac{c_e}{c_d} \frac{\tau - \tau_c}{\rho_s V_s^2}. \tag{14}$$

This equation predicts in particular a linear dependence of n with the bed shear stress $(\tau - \tau_c)$. It can be rewritten in terms of the Shields number,

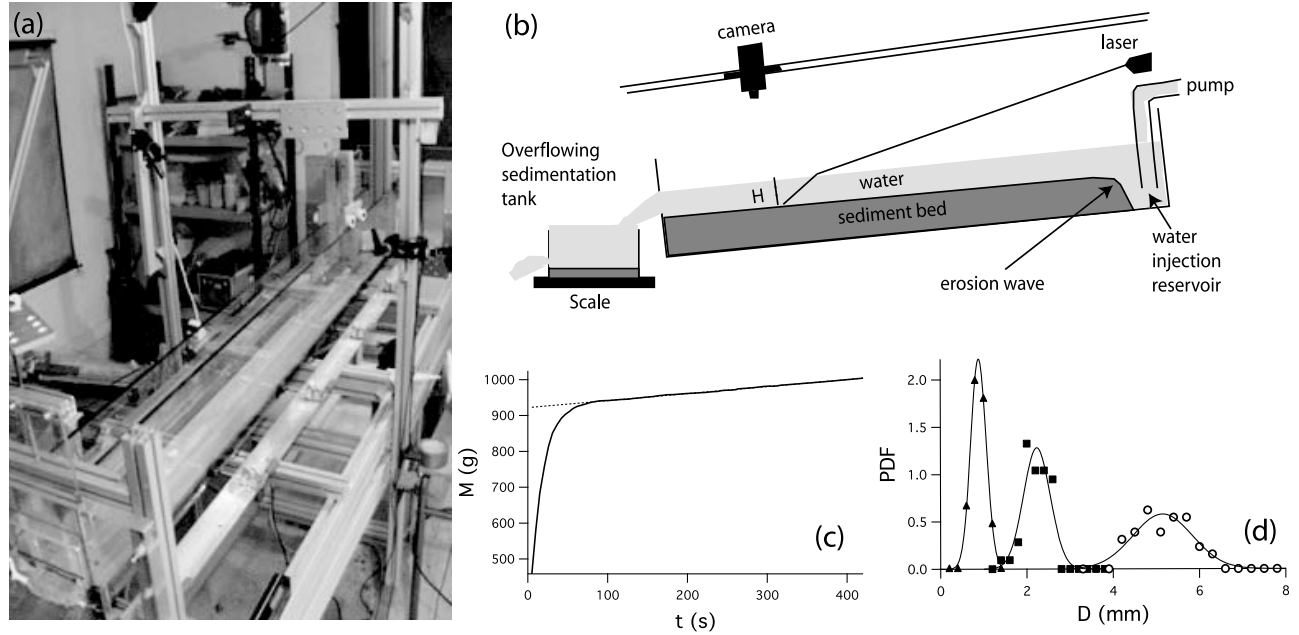$$n_{sat}D^2 = \frac{c_e}{c_d}(\tau^* - \tau_c^*). \tag{15}$$

In this saturated regime, the sediment flux corresponds to the saturated value,

$$q_{sat} = \delta v \, n_{sat} V, \tag{16}$$

with the particle density n_{sat} given by (15) and the velocity V by (13).

2.2. Steady Flow Over Varying Topography

[20] The second situation of interest is that of steady flow over varying topography. Then, assuming that the

Figure 2. (a) Photo and (b) schematics of the experimental setup. (c) Example of the cumulated sediment mass recorded as a function of time at the flume outlet. (d) Size distribution of the grains for series 1 (triangles), 2 (squares), and 3 (circles).

particles have negligible inertia so that their velocity V adapts instantaneously to the shear stress, the erosion-deposition equation (8) gives the following relaxation equation for the particle flux q_s:

$$\ell_d \frac{\partial q_s}{\partial x} = q_{sat} - q_s, \tag{17}$$

where

$$\ell_d = V t_d \tag{18}$$

is a deposition length. As shown below, this deposition length is closely related to the length traveled by a particle during one flight. It can be noted that this equation has the same form as that proposed by *Andreotti et al.* [2002], but with a different saturation length.

[21] As stated in section 1, one objective of the experiments presented below is to test the consistency of the above model and determine the involved coefficients: a and V_c for the velocity and c_d and c_e for the erosion and deposition rates. For the sake of simplicity, the settling velocity will be taken as $V_s = \sqrt{RgD}$, which amounts to neglecting the weak dependence of the drag coefficient with the Reynolds number (the numerical value of $\sqrt{RgD}$ corresponds to the settling velocity of a sand grain of diameter 0.65 mm in water).

3. Experimental Apparatus and Procedure

3.1. Setup

[22] The experiments were carried out in a rectangular inclinable flume of width $W = 9.6$ cm and length 240 cm (Figure 2a) partially filled with an erodible bed of quartz grains of density $\rho_s = 2650$ kg m^{-3} ($R = 1.65$). An experiment was started by preparing a flat bed of sediment of thickness

several centimeters (typically 10 cm). The sediment bed was flattened by sweeping a rake, whose tilt and height were constrained by two rails parallel to the channel. The bed slope S was measured with a digital inclinometer with accuracy 0.1°. Once the bed was ready, water was injected by a pump at the upstream flume inlet with constant discharge $W q_w$, where q_w is the discharge per unit width, measured with a flowmeter (accuracy 0.01 L min^{-1}). To prevent any disturbance of the bed, water was not injected as a point source but rather it overflowed smoothly onto the flume bed via a small reservoir (see Figures 2a and 2b). The reservoir extended across the full width of the channel and therefore guaranteed a uniform flow injection across the channel width. For all runs the discharge was high enough for the flow to fill the whole width of the flume.

[23] At the flume outlet, particles transported by the flow settled out in an overflow tank with constant water level. The tank rested on a high-precision scale (accuracy 0.1 g) connected to a computer that recorded the weight every ten seconds. The sediment discharge per unit river width q_s was deduced from the sediment cumulative mass. Figure 2c shows the mass of sediment accumulated in the overflow tank as a function of time during a typical experimental run. The initiation of the flow was followed by a transitory phase during which the mass of sediment collected at the flume outlet increased rapidly. After about two minutes, a steady state was reached characterized by a linear increase in the cumulative sediment mass with time indicating a constant sediment discharge (Figure 2c). All the measurements described hereafter were performed during this steady state regime and as long as the bed was flat. Our experiments correspond therefore to the case of a steady and uniform flow above a flat topography.

Table 3. Range of Parameters Explored for Each Series of Experiments

Series	D (mm)	S	Re_s	τ^*	Re^*	H/D	τ_c^*	Symbol
1	1.15	0.0017–0.07	156.9	0.006–0.24	12–77	7–10	0.016 ± 0.03	triangle
2	2.24	0.01–0.068	426.5	0.02–0.15	65–179	4–6	0.023 ± 0.002	square
3	5.50	0.04–0.12	1646	0.037–0.096	317–510	1.5–2	0.037 ± 0.001	circle

[24] Because we did not feed sediment at the flow inlet, an erosion wave slowly propagated from the inlet toward the outlet of the flume. All our experiments were stopped well before this degradation wave had reached the middle of the flume where the measurements were performed, so that this wave never interfered with our results. At the end of each experimental run, the slope of the flume bed measured at several locations all along the channel using the digital inclinometer was indeed equal to the initial slope, within the experimental precision.

[25] The water depth H was measured from the deviation of a laser sheet, as sketched in Figure 2b, with precision of ±1 mm. This depth was found to be constant along the section of the flume within the experimental precision. Assuming that the depth-averaged flow velocity was uniform in the spanwise direction, this velocity was given by $U = q_w/H$, with precision of 10%.

[26] The influence of the grain size, and therefore Re_s, on sediment transport was investigated by performing three series of experiments, each of them involving a bed of quartz grains of different granulometric distribution plotted in Figure 2d. D_{10}, D_{50} and D_{90} were equal to 0.94, 1.15 and 1.4 mm for the first series of experiments; 1.92, 2.24 and 2.6 mm for the second ones; and 4.52, 5.5 and 6.7 mm for the third ones, respectively. The bed granulometric distribution was therefore rather peaked around D_{50} for each series of experiments. As a result, our experiments avoid complex effects usually associated with an extended granulometric composition.

3.2. Characterization of the Flow

[27] For each series of experiments, 8 to 15 runs were performed with bed slopes ranging from 0.2° to 6° and water discharges ranging from 2 to 32 L min^{-1} (see Table 3). The corresponding flow Reynolds number $Re = q_w/\nu$ varied between 1500 and 6000, well above the threshold of transition from laminar to turbulent flow (which is of the order of 500 in open channel flows [Allen, 1985; Lajeunesse et al., 2010]). In all our experiments, the flow was therefore turbulent. The particle Reynolds number Re_*, which measures the ratio of the bed roughness to the thickness of the viscous sublayer, varied in the range 12 to 500 allowing us to explore both the transitional and the hydraulically rough regime. Finally, H/D varied in the range 2 to 10 which crosses the transition from "roughness layer" dominated to "deep" flows (at $H/D = 4$, approximately) (see Table 3).

[28] The vertical velocity profile of the flow was measured for several experimental runs using the Particle Imaging Velocity (PIV) method [Adrian, 1991]. Neutrally buoyant tracers (hollow glass beads) were introduced in the flow and illuminated by a vertical laser sheet. Side-view images of the flow were acquired using a high-speed camera (1000 frames per second, 1024 × 1024 pixels). The size of the imaged zone was chosen to be slightly larger than the maximum length traveled by the tracer particles between two images. The

images were processed to compute the instantaneous velocity fields. The time-averaged velocity field was then determined by averaging over 100 consecutive instantaneous fields (convergence was achieved after 40 fields).

[29] The profile of the time-averaged streamwise velocity was found to satisfy the logarithmic law

$$u(z) = \frac{u^*}{\kappa} \ln\left(\frac{z}{z_0}\right), \tag{19}$$

where z is the distance above the bed, $\kappa = 0.41$ is the Von Kàrmàn constant, and z_0 is the hydrodynamic roughness. An example of velocity profile is shown in Figure 3a. In that case, a fit of the profile with equation (19) leads to $u^* = 24 \pm 2$ cm/s and $z_0 = 4.1 \pm 0.5 \ 10^{-3}$ mm $\approx D/28$, a value typical of the hydraulically rough regime.

3.3. Shear Stress Exerted on the Sediment Bed

[30] The flow depth being uniform, the streamwise bed shear stress can be approximated by

$$\tau = \rho g R_h S, \tag{20}$$

where $R_h = HW/(2H + W)$ is the hydraulic radius. From equation (20), it follows that the Shields number and the shear velocity are respectively given by
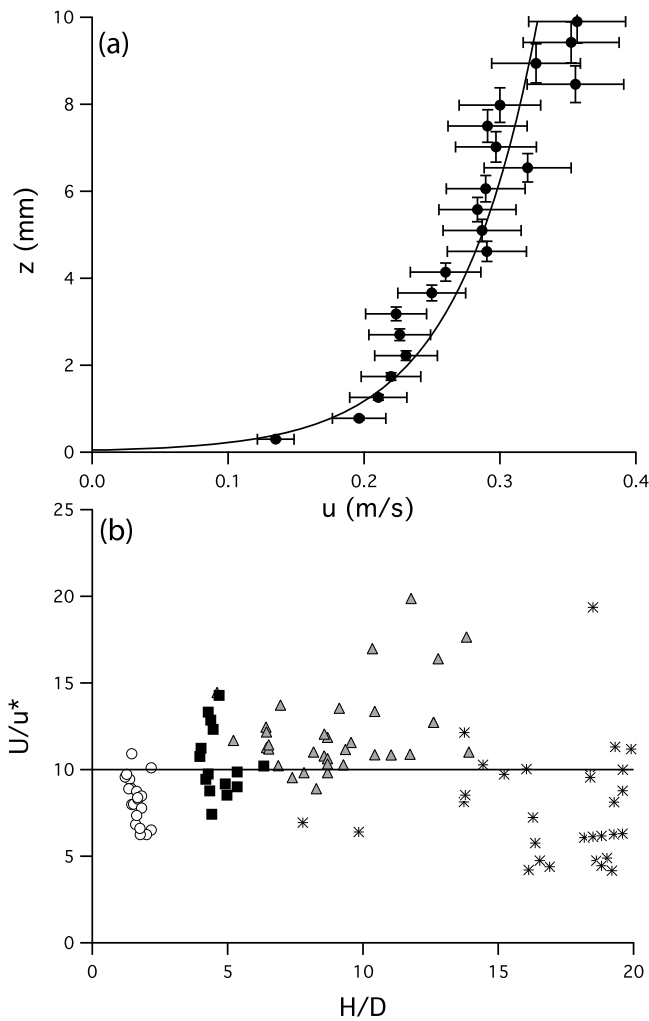
$$\tau^* = \frac{R_h S}{RD} \tag{21}$$

$$u^* = \sqrt{\frac{\tau}{\rho}} = \sqrt{gR_h S}. \tag{22}$$

Note that for the run shown in Figure 3a, the shear velocity calculated from equation (22) leads to $u^* = 28$ cm s^{-1}, which is close to the value $u^* = 24$ cm s^{-1} obtained by fitting the velocity profile with equation (19), ignoring the small side-wall corrections related to the large aspect ratio W/H.

[31] Our experimental setup does not permit simultaneous measurements of the flow velocity and bed load particle velocity. For this reason, τ^* and u^* were estimated in the following from the measurements of H and S using equations (21) and (22). The Chézy coefficients $C_z = U/u^*$ calculated for each run are plotted as a function of the ratio H/D in Figure 3b. Interestingly, we find $C_z \approx 10$, which is close to the measured value in many natural rivers as illustrated by the field data plotted in Figure 3b.

3.4. Characterization of the Motion of the Particles

[32] Under the action of the flow, a fraction of the bed particles were put into motion. They moved following intermittent trajectories composed of a succession of periods of rest and periods of motion as discussed in more detail in section 4. Bed load was the sole mode of sediment transport in our flume; we never observed any suspended load, as

Figure 3. (a) Vertical velocity profile $u(z)$ for Series 1, with $\tau^* = 0.041$, $Re_s = 156.9$, $H/D = 8$, $H/W = 0.1$, and $S = 0.0087$. The plain curve represents the logarithmic fit of the data. (b) Chézy coefficients $C_z = U/u^*$ as a function of H/D for Series 1 (triangles), 2 (squares), and 3 (circles). Stars represent field data measured in four rivers (North Saskatchewan River, Elbow River, Oak Creek, and Sagehen River) and extracted from the databases of *Brownlie* [1981] and *Bagnold* [1980].

expected for the range of Rouse number $R_o = V_s/\kappa u^* \propto 1/\sqrt{\tau^*}$ explored in our experiments (R_o was varied between 5 and 30).

[33] A high-speed camera (250 frames per second, 1024 × 1024 pixels) positioned vertically above the bed was used to track the motion of the sediment particles. About 10% of these were dyed black. This allowed us to track their position from frame to frame, with time resolution of 0.04 s, using a particle tracking algorithm. The data were then processed to calculate the streamwise and transverse particle velocities. The spatial resolution was such that the particle diameter was about 50 pixels and the size of the field of view of the order of 20 × 20 particle diameters. With these conditions, we were able to determine the position of the center of mass of a particle on an image with a precision of 0.05 mm.

However the oscillations of the water surface, which are the main source of experimental error, degraded the accuracy of these measurements by causing an apparent movement of particles at rest. The corresponding false velocities were calibrated for each experimental run by computing this apparent velocity. This allowed definition of a cutoff velocity in the range 10–30 mm s^{-1}, depending on the water flow rate, below which the particle was considered to be at rest (i.e., the velocity measurement was not taken into account).

[34] The same particle tracking algorithm was used to compute the lengths and durations of the particle flights. However, the size of the field of view had to be increased to 177.3 × 85.6 mm^2 in order to remain much larger than the characteristic particle flight length. The camera recorded the motion of the particles from above, not from the side of the flume. Measurements of the vertical velocity component and of the saltation height were therefore not feasible.

[35] Finally the surface density of moving particles was measured for each experimental run by counting manually the total number of particles (whether dyed or not) moving between two successive frames within the field of view, and averaging over a sufficiently large number of frames for the mean to converge. As mentioned above, a resting grain may appear to be in motion because of the slight oscillations of the water surface. However, such an apparent displacement fluctuates around zero and exhibits as many negative as positive values. This is not the case if the particle actually moves. To determine reliably whether a particle is at rest or not, we correlated the displacement of each examined particle on several images.
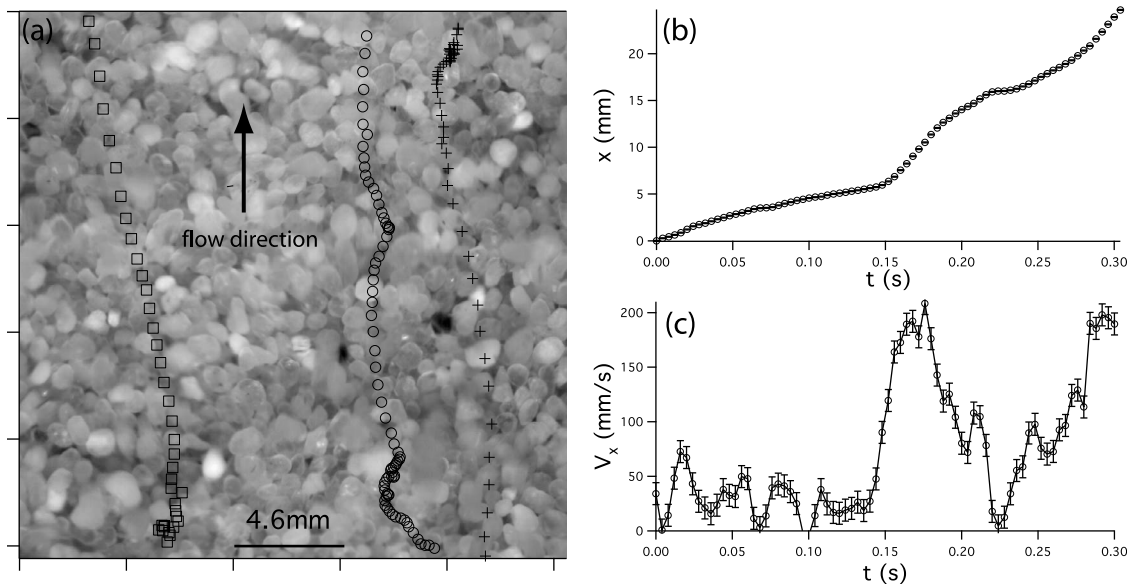
4. Experimental Results

[36] A sample of trajectories of the moving grains is shown on Figure 4a. The position along the streamwise x axis and the streamwise velocity component of one of the grains are also plotted as a function of time in Figures 4b and 4c. These data are representative of the general observations. Only a small fraction of the sediment bed particles is entrained by the flow. These bed load particles exhibit intermittent behavior: periods of motion, called "flights" and characterized by a highly fluctuating velocity, alternate with periods of rest.

4.1. Surface Density of Moving Particles

[37] Let us first focus on the surface density of moving particles n. Our observations show that, for each of the three series, n vanishes below a well-defined threshold value of the Shields number τ^*, and increases linearly with τ^* above the threshold value. It seems therefore natural to define the critical Shields number τ_c^* from this threshold value below which n vanishes.

[38] A linear fit of n versus τ^* leads to the values of τ_c^* reported in Table 3 and plotted in the inset of Figure 5. Not surprisingly, these values coincide with those deduced from direct measurement of the sediment flux using the scale at the flume outlet. They are consistent with the threshold values reported by other investigators (see the compilation by *Buffington and Montgomery* [1997]) which vary in the range $0.012 < \tau_c^* < 0.05$ within the range $20 < Re_* < 320$ corresponding to the inception of motion in our experiments. As shown in Figure 5, they are also close to the values predicted from the Brownlie correlation [*Brownlie*, 1981].
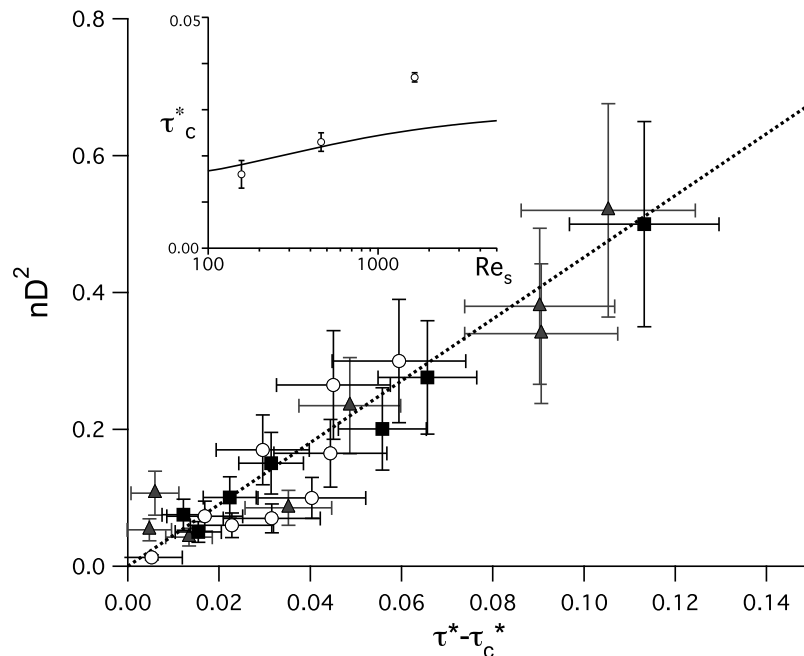
Figure 4. (a) Trajectories of three moving grains for Series 2, with $\tau^* = 0.057$, $H/D = 5$, $Re_s = 426.5$, and $S = 0.017$. The time interval between each point is 0.004 s. (b) Streamwise position and (c) streamwise velocity of one of these grains (corresponding to the circles) plotted as a function of time.

[39] The surface density n is plotted as a function of $(\tau^* - \tau_c^*)$ in Figure 5. It can be seen that the measurements obtained for the three series of experiments corresponding to the three grain sizes investigated in this paper (see Table 3) reasonably collapse onto the line corresponding to the linear relation
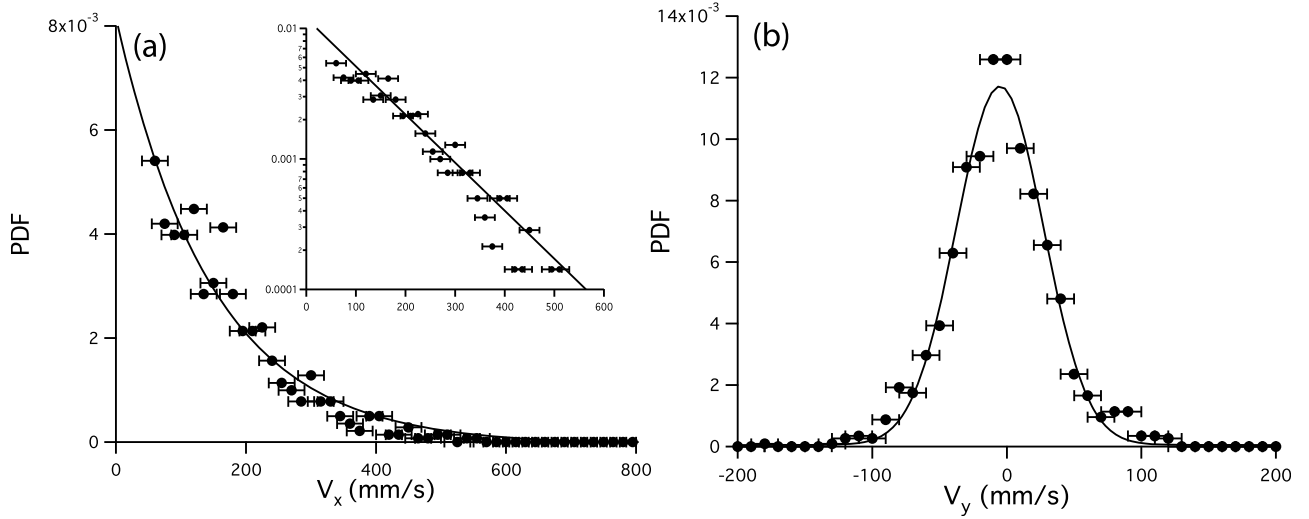
$$nD^2 = (4.6 \pm 0.2)(\tau^* - \tau_c^*). \tag{23}$$

4.2. Velocity Distribution of Bed Load Particles

[40] We now turn to the determination of the velocity distribution of the moving particles. To this end, we measured the instantaneous values of the streamwise and transverse velocity components, V_x and V_y, of all the dyed particles in motion within the field of view. This was achieved by identifying the particles moving between two successive frames, computing their velocities (see section 2) and stacking over

Figure 5. Graph showing nD^2 versus $(\tau^* - \tau_c^*)$. Triangles, squares, and circles correspond to Series 1, 2, and 3, respectively. Dashed line is the linear fit of the data. Inset shows critical Shields stress τ_c^* as a function of Re_s. Solid line is the Brownlie correlation [Brownlie, 1981].

Figure 6. (a) Experimental probability density functions (PDFs) of V_x for $\tau^* = 0.103$, $Re_s = 426$, $H/D = 5$, and $S = 0.042$. Inset shows the same data represented on a semilog plot. (b) Corresponding PDFs of V_y.

a suitable number of frames for convergence. This method requires a suitable definition of a moving particle, taken as one with velocity greater than the cutoff velocity defined in section 2. Several thousands of velocity measurements were thus performed for each experiment, allowing us to estimate experimentally the probability density functions (PDF) of V_x and V_y, samples of which are shown in Figure 6. Note that these distributions concern only the moving particles, i.e., those with velocity larger than the cutoff velocity. If the resting particles were taken into account, the distribution would of course exhibit a sharp and discontinuous peak at $V = 0$ because the number of particles at rest far exceeds that of moving grains.

[41] For the explored range of parameters, the PDFs of V_x were found to decrease monotically to zero (Figure 6a) and are well fitted by the exponential law

$$P(V_x) = \frac{1}{V} e^{-V_x/V}, \qquad (24)$$

where V is the averaged streamwise particle velocity.

[42] As a first approximation, the PDFs of V_y are reasonably well fitted by a Gaussian function centered on zero, as shown in Figure 6b,

$$P(V_y) = \frac{1}{\sqrt{\pi}\delta V_y} e^{-\left(\frac{V_y}{\delta V_y}\right)^2}. \qquad (25)$$

The average transverse velocity component is 0, which is consistent with a particle trajectory mainly oriented along the flow direction. The width of the Gaussian δV_y characterizes the order of magnitude of the velocity fluctuations along the y axis and reflects the stochastic deviations of the particle off the main streamwise motion due to their interactions with the rough bed of sediment. These deviations are, on average, symmetric with respect to the main flow direction. The ratio $\delta V_y/V$ is plotted as a function of $(u^* - u_c^*)/V_s$ in Figure 7a. It ranges between 0.2 and 1 and decreases when τ^* increases; however, the trend is vague. Finally, a closer examination of

Figure 6b suggests that the tails of the PDFs of V_y are thicker than Gaussian. This result is consistent with the model of *Ganti et al.* [2010], suggesting that the particles spread along the y axis following an anomalous diffusion process.

[43] Interestingly these results are identical to those obtained by *Charru et al.* [2004] for bed load particles entrained by a viscous flow, not turbulent. This suggests that particle motion is dominated by the mean value of the bed shear stress, and that fluid velocity fluctuations are not important. However, this conclusion might be wrong very near the threshold in the fully rough regime ($\tau^* \approx \tau_c^*$, $Re_* > 70$), where turbulent bursts may maintain a small particle transport rate.

[44] For each experimental run, the mean particle velocity V was computed from the PDF of V_x using equation (24). As shown in Figure 7b, measurements of the dimensionless velocity V/V_s converge onto a single line when plotted as a function of $(u^* - u_c^*)/V_s$. Thus the particle velocity can be written
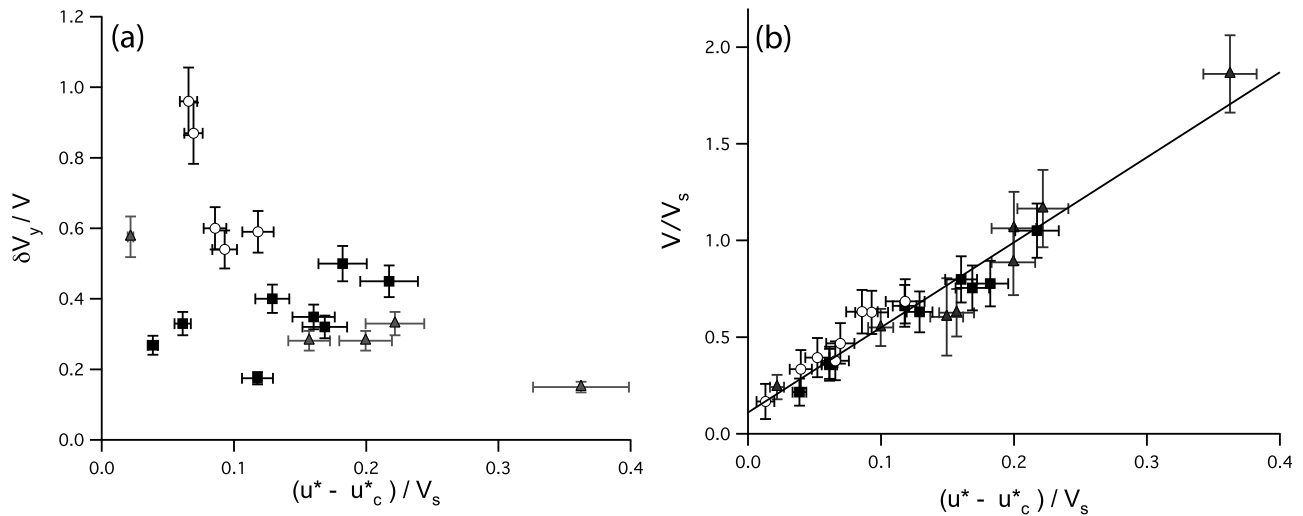
$$\frac{V - V_c}{V_s} = a \frac{u^* - u_c^*}{V_s}, \qquad V_s = \sqrt{RgD}, \qquad (26)$$

which is identical to (13). Fitting the data, the slope a and the threshold velocity V_c are found to be

$$a = 4.4 \pm 0.2, \qquad \frac{V_c}{V_s} = 0.11 \pm 0.03. \qquad (27)$$

The above result suggests that the velocity is discontinuous at the threshold of sediment transport, particles moving there with a nonzero velocity V_c. This result is supported by the experimental observation that, close to the threshold, a particle, once dislodged from the sediment bed, does not stop immediately but may travel over some distance. It is also consistent with the hysteretic nature of the threshold of motion first evidenced by *Hjülstrom* [1935] and with observations of the motion of a single particle on a fixed bed by *Francis* [1973] and *Abbott and Francis* [1977].

[45] Although our data demonstrate unambiguously that a particle exhibits a nonzero velocity V_c, at the threshold of
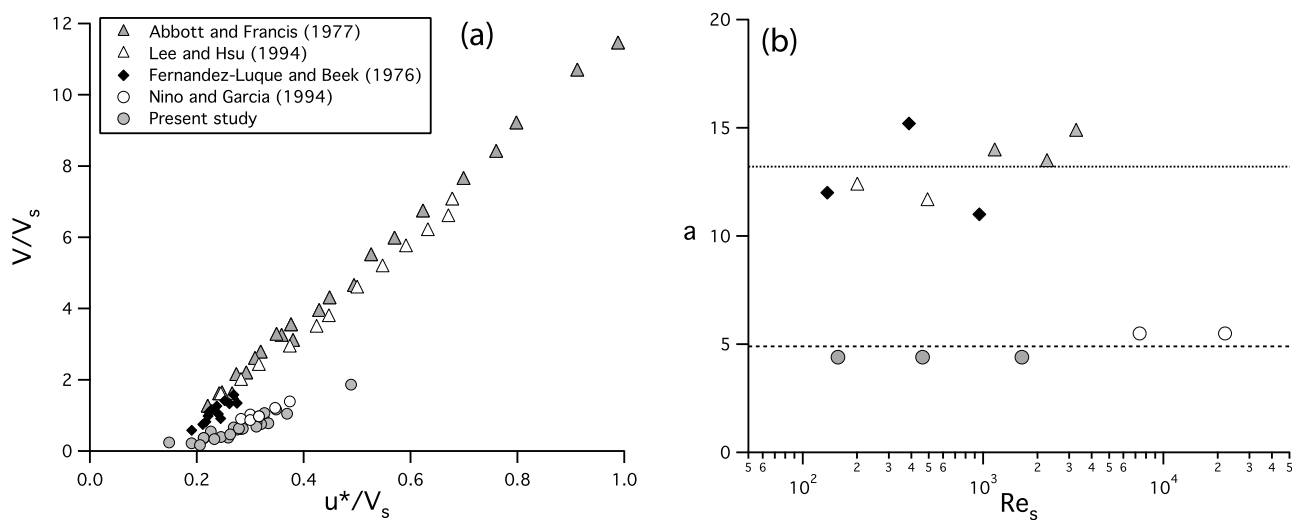
Figure 7. Graphs showing (a) $\delta V_y/V$ and (b) average particle velocity V/V_s as a function of $(u^* - u_c^*)/V_s$, with $V_s = \sqrt{RgD}$. Triangles, squares, and circles correspond to series 1, 2, and 3, respectively. Solid line represents linear fit of the data.

sediment transport, determining this velocity precisely remains an experimental challenge. V_c is indeed extremely sensitive to the definition of τ_c^*: a 10% change of τ_c^* results in a 30% change of V_c. The difficulty to precisely estimate τ_c^* might explain the important differences between the values of the coefficient b of equation (7) available in the literature (see Table 2).
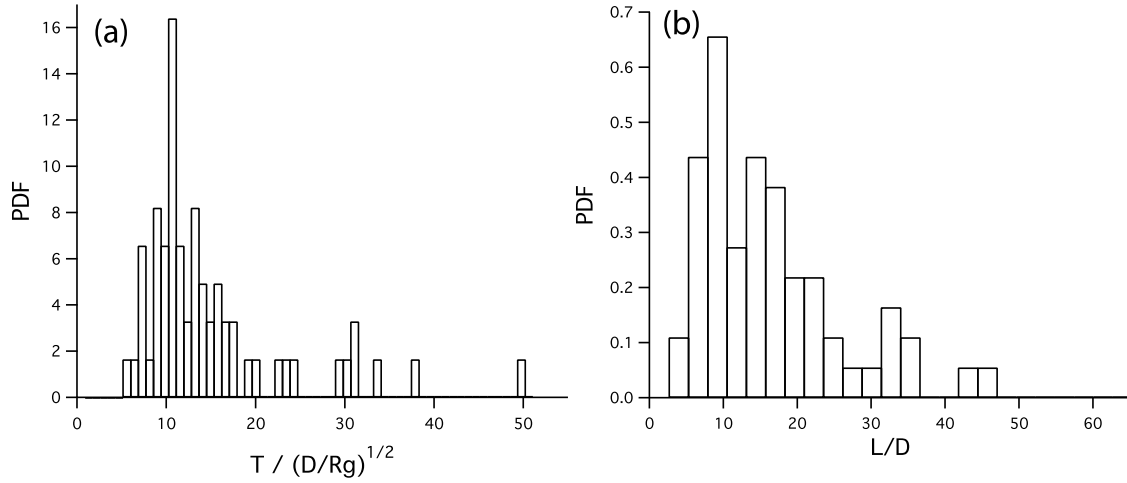
[46] Our particle velocity measurements are compared to ones from four previous investigations in Figure 8a where V/V_s is plotted as a function of u^*/V_s (unfortunately, the value of u_c^* was not available for several data sets, preventing us from plotting the data as a function of $(u^* - u_c^*)/V_s$). Two of these data sets were obtained by tracking the motion of a

single grain moving above a rigid nonerodible rough bed [*Lee and Hsu*, 1994; *Abbott and Francis*, 1977]. The other ones, including the present study, correspond to erodible beds [*Fernandez-Luque and Van Beek*, 1976; *Nino and Garcia*, 1994]. Each of these authors performed several series of experiments working with different grain sizes and densities so that, altogether, these data span the range 100–22,000 for Re_s and 0.01–1 for τ^*.

[47] Figure 8a shows that V/V_s increases linearly with u^*/V_s for each series of data in accordance with equation (26). A fit of each series of data by this equation allows the computation of the coefficient a. The results are displayed in Figure 8b. Two different trends are visible depending on the

Figure 8. (a) Average particle velocity V/V_s versus u^*/V_s measured by various authors (see the legend on the graph). The data of *Abbott and Francis* [1977] and *Lee and Hsu* [1994] correspond to the case of a single grain moving above a rigid rough bed. Those of *Fernandez-Luque and Van Beek* [1976], *Nino and Garcia* [1994], and the present study correspond to an erodible bed. (b) Velocity coefficient a as a function of Re_s. The symbols are identical to the one used in Figure 8a.

Figure 9. (a) PDF of flight durations normalized by $\sqrt{D/Rg}$. (b) PDF of flight lengths normalized by D. Parameters are $D = 1.15$ mm (series 1), $\tau^* = 0.06$, $H/D = 9$, $Re_s = 156.9$, and $S = 0.01$.

nature of the bed. For a single grain entrained above a rigid rough bed [*Abbott and Francis*, 1977; *Lee and Hsu*, 1994], $a = 13.2 \pm 0.6$ within the explored range of Re_s ($130 < Re_s < 3200$). In the case of an erodible bed (data of *Nino and Garcia* [1994] and the present study), $a = 5.0 \pm 0.6$ for an even larger range of Re_s ($160 < Re_s < 22000$). To summarize, particles entrained by the flow move more slowly above a mobile bed than above a rigid one.

[48] This observation is apparently contradicted by the data of *Fernandez-Luque and Van Beek* [1976]. Indeed, although these data correspond to an erodible bed, they are much closer to those for a noneerodible bed (Figure 8a). A plausible explanation is that *Fernandez-Luque and Van Beek* [1976] estimated the average particle velocity from the time required by the particles to cover a fixed distance. This method is likely to ignore movements smaller than this fixed distance and may therefore bias the data. Indeed, as noted by the authors themselves [*Fernandez-Luque and Van Beek*, 1976, p. 135], "we obviously followed those particles that were carried in suspension at almost the same velocity and not those particles that were just being eroded and had a much lower transport velocity."

4.3. Characteristic Length and Duration of the Flights

[49] As already discussed, sediment particles exhibit an intermittent behavior composed of a succession of periods of motion or "flights" and periods of rest. Using particle tracking, we measured the durations T and the lengths L of these flights for all experimental runs. As described in section 3.4, the size of the observation window had to be increased in order to guarantee that it was larger than the maximum flight length recorded. These measurements had to be performed using a semiautomatic procedure allowing us to check manually that a given particle was correctly tracked from frame to frame. They were therefore time consuming and the number of data was not enough to obtain fully converged PDFs. Nevertheless, the histograms of T and L, examples of which are shown in Figure 9, exhibit well-defined peaks corresponding to the most probable flight duration $\langle T \rangle$ and flight length $\langle L \rangle$, respectively. We also note that the two histograms in Figure 9 are not symmetric but are

skewed toward long durations and lengths so that the mean is slightly larger than the most probable value.

[50] The most probable flight durations $\langle T \rangle$, normalized by the characteristic settling time $D/V_s = (D/Rg)^{1/2}$, are plotted in Figure 10a. The dimensionless settling time varies typically between 7 and 12, with no clear variation with either $(u^* - u_c^*)/V_s$ or Re_s. A fit of the data leads to

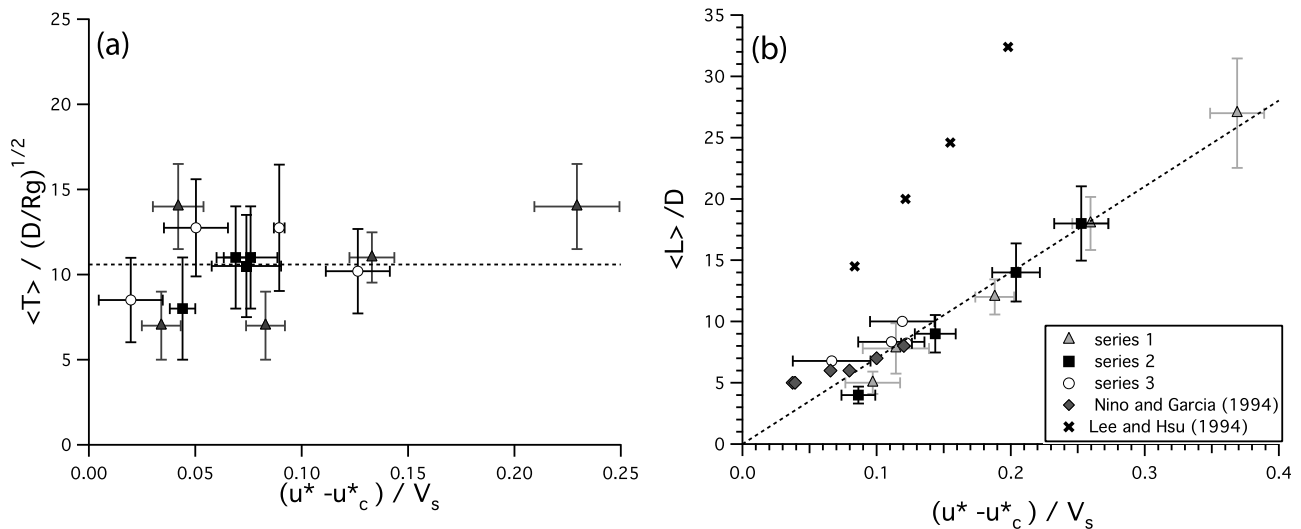$$\frac{\langle T \rangle}{\sqrt{D/Rg}} = 10.6 \pm 0.7. \tag{28}$$

[51] Turning to the most probable flight length, Figure 10b shows that it increases with the shear velocity according to the linear relation

$$\frac{\langle L \rangle}{D} = (70 \pm 2) \frac{u^* - u_c^*}{V_s}, \tag{29}$$

with no significant dependence of the numerical coefficient on Re_s for the range investigated in this paper (namely $150 < Re_s < 1650$).

[52] Table 2 summarizes the results of previous investigations by *Fernandez-Luque and Van Beek* [1976], *Abbott and Francis* [1977], *Sekine and Kikkawa* [1992], *Nino and Garcia* [1994], *Lee and Hsu* [1994], and *Hu* [1996]. Although these authors come to different predictions, all but *Fernandez-Luque and Van Beek* [1976] report an increase of $\langle L \rangle/D$ with τ^* or equivalently u^*. The reason why the results of *Fernandez-Luque and Van Beek* [1976] are different is that they calculated the average flight length from the cumulative distribution over their whole data sets, which included several flow rates; such a calculation cannot, of course, evidence any variation of flight length with u^*. Therefore, we ignore the results of *Fernandez-Luque and Van Beek* [1976] in the following.

[53] Among the remaining studies, only *Nino and Garcia* [1994] and *Lee and Hsu* [1994] provide the values of u_c^* that allow direct comparison with our data. *Nino and Garcia* [1994] performed two series of experiments with beds composed of mobile sediments of sizes 15 and 31 mm (about ten

Figure 10. (a) Most probable flight duration, $\langle T \rangle / \sqrt{D/Rg}$, and (b) most probable flight length, $\langle L \rangle / D$, as a function of $(u^* - u^*_c)/V_s$. Dashed line shows linear fit. Triangles, squares, and circles correspond to series 1, 2, and 3, respectively. Diamonds represent data from *Nino and Garcia* [1994] for an erodible bed. Crosses represent data from *Lee and Hsu* [1994] for a single grain on a fixed rough bed.
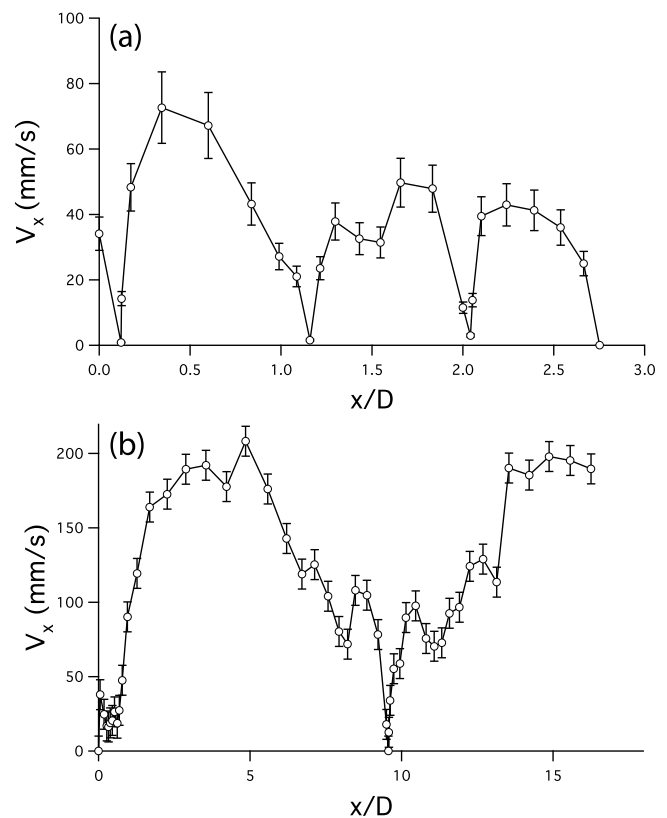
times as large as in our experiments), corresponding to Re_s equal to 7400 and 21,900, respectively. Their data plotted on Figure 10b exhibit a good agreement with our own measurements except for one data point for the smallest value of $u^* - u^*_c$, which stands above the regression line. This point is however close to the threshold and is therefore very sensitive to the exact value of u^*_c, which *Nino and Garcia* [1994] did not measure but deduced from the Shields curve. A less than 10% change of the value of u^*_c is enough to bring the data point in question back onto our experimental data trend. The results of *Nino and Garcia* [1994] are therefore in good agreement with our own observations, thus extending the validity of equation (29) to values of Re_s as far as 21,900.

[54] As for *Lee and Hsu* [1994], they investigated the case of a single particle entrained above a rigid rough bed. Their data plotted on Figure 10b appear to increase linearly with $u^* - u^*_c$ as predicted by equation (29). However the flight lengths reported for a single particle above a rigid bed are much larger than in the case of a mobile bed. This observation is consistent with the fact that particles move faster above a rigid bed than above a mobile one as discussed in section 4.2.
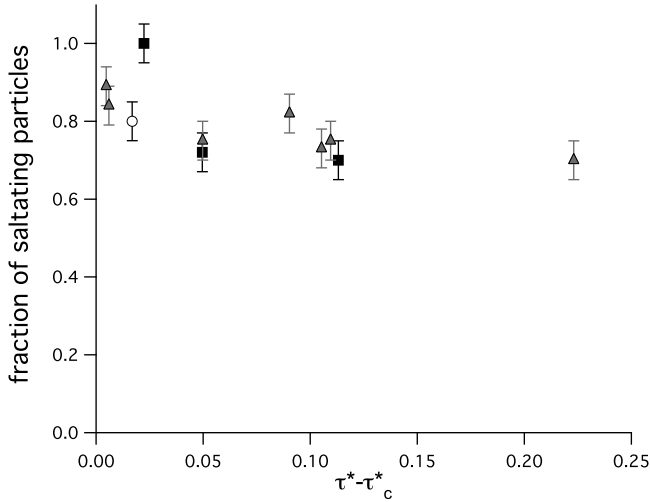
4.4. Rolling and Saltation

[55] The experimental results presented up to now, including flight lengths and durations, have been discussed without distinction of the kind of motion, rolling, sliding or saltation, of the particles. Thanks to the high spatial and temporal resolutions, two different kinds of motion can be distinguished by plotting the instantaneous velocity V_x of a particle as a function of its position x, as shown in Figure 11.

[56] The first type of motion corresponds to rolling. It involves particles that strongly interact with the bed. As shown in Figure 11a, their motion is characterized by small velocities (typically $V_x < 100$ mm s^{-1}) which vary as a function of x with a periodicity on the order of the grain size D. The variations are almost symmetrical with an acceleration phase roughly equal to the deceleration phase.

Figure 11. Streamwise velocity component as a function of the downstream coordinate x for (a) a rolling particle and (b) a saltating particle. These data were obtained during the same experimental run with $D = 2.24$ mm (series 2), $\tau^* = 0.057$, $H/D = 5$, $Re = 426.5$, and $S = 0.017$. Note the change of scale, particularly along the x axis, between the two plots.

Figure 12. Proportion of bed load particles moving by saltation as a function of ($\tau^* - \tau_c^*$). Triangles, squares, and circles correspond to the experimental series 1, 2, and 3, respectively.

Direct observations confirm that these particles remain in nearly persistent contact with the bed. The observed periodicity clearly reflects the length scale of the bed roughness, on the order of the grain size.

[57] Saltation, the second kind of motion, is illustrated in Figure 11b. It is characterized by much longer flights with a short phase of large acceleration (up to 0.9 g on a typical distance on the order of D) and a longer phase where the velocity decreases more slowly. Saltation involves fast particles (typically $V_x > 100$ mm s^{-1}) traveling sufficiently high above the bed for their trajectories not to be perturbed by the bed roughness.

[58] Recall that we did not perform systematic measurements of the motion of the particles from the side of the flume. The distinction we establish between rolling and saltation is therefore primarily based on the shape of the V_x versus x curves. However, we consider that our interpretation is supported by the results of *Charru et al.* [2007], who investigated experimentally the trajectories of a few particles entrained by a laminar flow above a rough bed. They recovered the same two distinctive V_x versus x types of curve as in our experiments. Using two cameras, which allowed them to observe the particle trajectories from both above and the side of the flume, they demonstrated that V_x versus x curves similar to those displayed in Figure 11a do correspond to rolling, whereas trajectories of the type shown in Figure 11b correspond to saltation.

[59] Finally, let us note that direct observation shows that during one flight, the same particle may undergo phases of rolling and phases of saltation. The proportion of saltating or rolling particles was measured by counting the total number of dyed particles rolling between two successive frames, comparing this number to the total number of moving dyed particles, and averaging over a sufficient number of frames. A particle was considered to be rolling if its velocity plotted as a function of x presented the same kind of oscillations as in Figure 11a. The results, plotted in Figure 12, indicate that the sediment transport is strongly dominated by saltation,

which represents from 70% to 100% of the particles in motion. In particular, the proportion of saltating particles remains high close to the threshold of sediment transport. This observation contradicts the commonly accepted scenario according to which the majority of particles are rolling and sliding for $\tau^* \approx \tau_c^*$ and saltation progressively becomes the dominant mode of motion as τ^* increases [*Van Rijn*, 1984].

5. Summary and Discussion

[60] Let us summarize our experimental results on the motion of bed load particles in a steady and uniform turbulent flow above a flat topography. In this equilibrium, or saturated, regime, the erosion and deposition rates balance each other. Our observations show that the particles entrained by the flow exhibit an intermittent behavior composed of a succession of periods of motion with a highly fluctuating velocity, called "flights," and periods of rest. During one flight, a particle may successively go through phases of rolling and sliding (a kind of motion also called reptation in studies of aeolian transport) during which it moves in nearly persistent contact with the rough bed, and phases of saltation, during which it travels sufficiently high above the bed to reach high velocities. Our main quantitative results are divided into six parts: (1) threshold, (2) density of moving particles, (3) particle velocity distributions, (4) mean particle velocity, (5) flight duration, and (6) flight length.

[61] 1. Particles begin to move at Shields stress larger than a threshold τ_c^*, which was determined from the extrapolation to zero of the surface density of moving particles. This threshold was found to be in agreement with previous results in the explored range of sedimentation Reynolds number, $160 < Re_s < 1650$ (see Table 3 and the inset of Figure 5).

[62] 2. Above the threshold, the number of moving particles per unit bed area, n, increases linearly with $\tau^* - \tau_c^*$ (see equation (23) and Figure 5). This result is consistent with the erosion-deposition model presented in section 2. From the identification of the measured density (23) with the saturated density (15) predicted by the model, the ratio of the erosion and deposition coefficients is found to be

$$\frac{c_e}{c_d} = 4.6 \pm 0.2. \tag{30}$$

This ratio has no significant dependence on the settling Reynolds number. The linear dependence of nD^2 on $\tau^* - \tau_c^*$ is also consistent with the indirect measurements performed by *Fernandez-Luque and Van Beek* [1976], who found a lower coefficient 1.8 for $\tau^* - \tau_c^* < 0.1$. As mentioned in section 2, another erosion time could be defined on dimensional grounds, $t_e = D/(u^* - u_c^*)$, instead of the acceleration time defined by the momentum balance (12). This choice would lead to $n \propto u^* - u_c^*$, which clearly does not agree with the measurements reported in Figure 5.

[63] 3. The experimental PDFs of longitudinal and transverse particle velocities in a turbulent flow obey a decreasing exponential law and a Gaussian law, respectively (see Figure 6). This result is similar to the observations of *Charru et al.* [2004] for viscous flows. This similarity suggests that particle motion is dominated by the mean value of the bed shear stress, and that the particle velocity distributions are largely independent of the fluid velocity fluctuations.

[64] 4. The dimensionless mean particle velocity V/V_s increases linearly with the dimensionless shear velocity $u*/V_s = \sqrt{\tau*}$, where $V_s = \sqrt{RgD}$ is a characteristic sedimentation velocity (see equation (26) and Figure 7b). The slope of the linear law and velocity at threshold are given by

$$a = 4.4 \pm 0.2, \qquad \frac{V_c}{V_s} = 0.11 \pm 0.03.$$

Again, no significant dependence was noted on the settling Reynolds number, which was varied in the range $157 < Re_s < 1646$. This velocity law fully agrees with equation (13), which arises from a simple force balance. The above value of the coefficient a is close to that of previous investigations, which found a in the range 4.4–5.5 for an even larger range of settling Reynolds number (see Figure 8). This coefficient is much lower than that over a rough nonerodible bed, which was found to be 13.2 ± 0.6 in the range $130 < Re_s < 3200$: Particles therefore move more slowly above a mobile bed than above a rigid one. This result shows that the effective friction coefficient on a moving bed is higher, or, in other words, that the momentum transfer to the bed is enhanced.

[65] 5. The distribution of the durations of particle flights exhibits a well-defined peak corresponding to the most probable duration $\langle T \rangle$ (see Figure 9a). Once normalized with the settling time D/V_s, $\langle T \rangle$ was found to be independent of both $\tau*$ and Re_s in the range of parameters explored (see equation (28) and Figure 10a). Identification of this flight duration with the settling time (10) introduced in the erosion-deposition model provides the following value for the deposition coefficient:

$$c_d = 0.094 \pm 0.006. \tag{31}$$

From this estimate of the deposition coefficient and equation (30) for the ratio c_e/c_d, the erosion coefficient is found to be

$$c_e = 0.43 \pm 0.05. \tag{32}$$

[66] 6. As for flight durations, the distribution of the lengths of particle flights exhibits a well-defined peak corresponding to the most probable length $\langle L \rangle$ (see Figure 9b). This most probable flight length, once normalized with the particle diameter D, increases linearly with $(u* - u_c*)/V_s$ (see equation (29) and Figure 10b).

[67] Finally, all the experimental results support the erosion-deposition model presented in section 2, and allow the calibration of the coefficients: the deposition coefficient involved in the deposition rate (9) is given by (31), the erosion coefficient involved in the erosion rate (11) is given by (32), and the velocity coefficients involved in the velocity law (13) are given by (27). Remarkably these four coefficient are constants: their dependence on the dimensionless parameters is too weak to be measured, within the experimental uncertainties and the range of parameters explored. In particular, they appear to be the same for the hydraulically smooth, transitional, and hydraulically rough regimes.

[68] From the above results, we can now determine the deposition length ℓ_d and the saturated particle flux q_{sat}

involved in the dynamical equation (17) for sediment transport over varying topography. Indeed, although the experiments reported here have been conducted under steady and spatially uniform flow conditions, ℓ_d and q_{sat} only depend on equilibrium quantities.

[69] The deposition length ℓ_d may be determined in two slightly different ways. The first one is to use its definition (18), $\ell_d = V t_d$, with the mean particle velocity given by (26) and the settling time given by (10). Hence,

$$\frac{\ell_d}{D} = \frac{1}{c_d} \frac{a(u* - u_c*) + V_c}{V_s}, \tag{33}$$

where, from (27) and (31), $a/c_d = 47$ and $V_c/c_d V_s = 1.2$. This law predicts that, at threshold, the flight length is on the order of one particle diameter, as expected; however, for practical purposes, the small additive constant $V_c/c_d V_s$ may be neglected. The second way is to identify the deposition length with the most probable flight length (29), giving

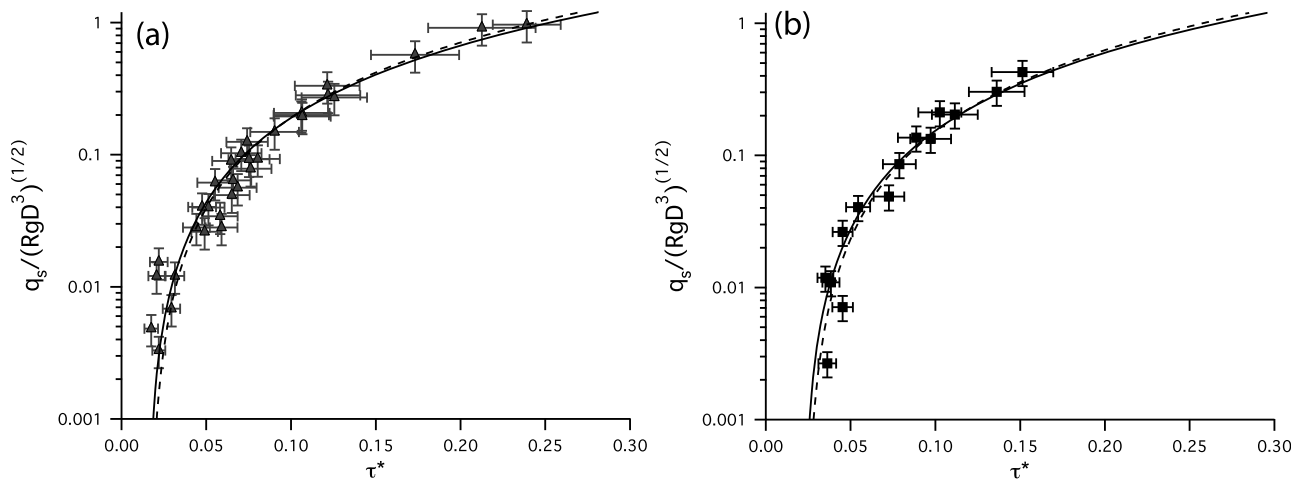$$\frac{\ell_d}{D} = 70 \frac{u* - u_c*}{V_s}. \tag{34}$$

Ignoring the small correction $V_c/c_d V_s$ in (33), the two estimations of ℓ_d are the same, except for the numerical coefficients which differ by about 40%. This difference reflects the fact that T, L and V are not independent stochastic variables, so that the most probable flight length $\langle L \rangle$ is not equal to the product $V\langle T \rangle$ of the mean velocity and the most probable flight time. Intuitively, we expect that longer flights correspond to particles reaching higher altitudes where the flow is faster. As a result, the PDFs of velocities should be correlated with the PDFs of flights durations, short flight durations corresponding to small velocities whereas long flight durations would correspond to larger velocities. Exploring this scenario would require the computation of the joint distribution of particle velocities and flight durations, which cannot be done with our too small data set.

[70] The determination of the saturated particle flux q_{sat} involved in the dynamical sediment transport law (17) is straightforward: it is the product of the surface density (23) of moving particles and the mean particle velocity (26). Hence,

$$\frac{q_{sat}}{\sqrt{RgD^3}} = 10.6(\tau* - \tau_c*)\left(\sqrt{\tau*} - \sqrt{\tau_c*} + 0.025\right). \tag{35}$$

The last numerical coefficient, although physically significant since it represents the nonzero particle velocity at threshold, may be neglected for practical purposes.

[71] Equation (35) for q_{sat} has been tested against direct measurements of the sediment transport rate at the flume outlet, performed with the scale (see section 3). Equation (35) does not involve any adjustable parameter (all the coefficients have been determined experimentally) and the measurements with the scale are independent of all the quantities measured from image acquisition (τ_c*, a, c_e, c_d, …). The scale measurements, along with the curve corresponding to equation (35), are shown in Figure 13 for series 1 and 2. It appears that the agreement is remarkable. Note that ignoring

Figure 13. Dimensionless transport rate $q_s/\sqrt{RgD^3}$ versus τ^* for (a) series 1 and (b) series 2. Points are measurements from the scale at the flume outlet. Solid lines represent equation (35), and dashed lines represent equation (35) with the last numerical coefficient set to zero.

the coefficient 0.025 in (35) (dashed line in Figure 13) has little effect.

6. Conclusion

[72] Up to now, the majority of the bed load transport laws proposed in the literature have been focused on the establishment of a relation between the local volumetric flow rate of particles and the local shear stress exerted by the fluid flow on the bed. These relations implicitly consider that the particle flux is in equilibrium with the shear stress, and consequently ignore any relaxation effect, although the latter is now recognized to control the development of bed forms, especially ripples [*Charru*, 2006].

[73] In order to overcome this limitation, *Charru et al.* [2004] developed an erosion-deposition model of bed load transport under viscous flow, which accounts for a relaxation effect related to the time needed for a particle to settle once it is entrained in the fluid flow. This model was shown to successfully predict the development of ripples and rhomboid patterns created by viscous flows [*Charru et al.*, 2004; *Devauchelle et al.*, 2010a, 2010b]. An extension of the model to turbulent flows was proposed by *Charru* [2006] (see section 2). However, despite the plethora of experimental investigations of bed load transport in turbulent flow, this model has not been tested so far, since measurements of the relevant quantities are either missing or inconsistent.

[74] The primary objective of this paper was to determine the coefficients of the erosion-deposition model for turbulent flows. To this end, we investigated the motion of bed load particles in a steady and spatially uniform turbulent flow above a flat bed of particles with uniform size. Using a high-speed video imaging system, we visualized the trajectories of the entrained grains and measured their velocity, the length and duration of their flights and the surface density of moving particles. As far as we know, this study is the first to achieve such measurements.

[75] The experimental results support the erosion-deposition model of *Charru* [2006] and allowed the calibration of the involved coefficients. These results confirm the idea that it is

the erosion rate which locally depends on the shear stress, not the sediment flux. The flux results from a local mass balance between advected, eroded and deposited particles. The turbulent erosion-deposition model needs now to be tested against the development of bed forms, ripples and dunes, as was done in the laminar case. This is a work in progress.

[76] Finally, note that the dynamics of the sediment transport in the immediate vicinity of the threshold remains an open problem. Here, the available measurements exhibit large scatter, as do the predictions of transport rate relations. Difficulties can be expected to arise not only from the hydrodynamics (the effect of turbulent bursts), but also from the geometry of the disordered bed. The preparation of the bed, and slow phenomena such as armoring, segregation on a polydisperse bed, or slow variations along the channel, are likely to be of importance. This analysis remains to be done.

References

Abbott, J., and J. Francis (1977), Saltation and suspension trajectories of solid grains in a water stream, *Philos. Trans. R. Soc. London A*, *284*, 225–254.

Adrian, R. (1991), Particle imaging techniques for experimental fluid mechanics, *Ann. Rev. Fluid Mech.*, *23*, 261–304.

Ahnert, F. (1970), Functional relationships between denudation, relief, and uplift in large mid-latitude drainage basins, *Am. J. Sci.*, *268*, 243–263.

Allen, J. (1985), *Principles of Physical Sedimentology*, Allen and Unwin, London.

Andreotti, B., P. Claudin, and S. Douady (2002), Selection of dune shapes and velocities—Part 2: A two-dimensional modelling, *Eur. Phys. J. B*, *28*(3), 341–352.

Ashida, K., and M. Michiue (1973), Studies on bed-load transport rate in open channel flows, in *Proceedings of the International Association for Hydraulic Research International Symposium on River Mechanics, 9–12 January 1973, Bangkok, Thailand*, pp. 407–417, Asian Inst. of Technol., Bangkok.

Bagnold, R. (1956), The flow of cohesionless grains in fluids, *Philos. Trans. R. Soc. London A*, *249*, 235–297.

Bagnold, R. (1973), The nature of saltation and of 'bed-load' transport in water, *Proc. R. Soc. London, Ser. A*, *332*, 473–504.

Bagnold, R. (1980), An empirical correlation of bedload transport rate in flumes and natural rivers, *Proc. R. Soc. London, Ser. A*, *372*, 453–473.

Braun, J., and M. Sambridge (1997), Modelling landscape evolution on geological time scales: a new method based on irregular spatial discretization, *Basin Res.*, *9*(1), 27–52.

Bridge, J. S., and D. F. Dominic (1984), Bed load grain velocity and sediment transport rates, *Water Resour. Res.*, *20*, 476–490.

Brownlie, W. (1981), Compilation of alluvial channel data: Laboratory and field, technical report, W. M. Keck Lab. of Hydraul. and Water Resour., Div. of Eng. and Appl. Sci., Calif. Inst. of Technol., Pasadena.

Buffington, J., and D. Montgomery (1997), A systematic analysis of eight decades of incipient motion studies, with special reference to gravel-bedded rivers, *Water Resour. Res.*, *33*, 1993–2029.

Carretier, S., and F. Lucazeau (2005), Response times in a mountain-piedmont system. Results of a numerical model, *Geophys. Res. Abstr.*, *7*, 03902.

Charru, F. (2006), Selection of the ripple length on a granular bed sheared by a liquid flow, *Phys. Fluids*, *18*, 121508, doi:10.1063/1.2397005.

Charru, F., and E. Hinch (2006), Ripple formation on a particle bed sheared by a viscous liquid. Part 1. Steady flow, *J. Fluid Mech.*, *550*, 111–121.

Charru, F., H. Mouilleron, and O. Eiff (2004), Erosion and deposition of particles on a bed sheared by a viscous flow, *J. Fluid Mech.*, *519*, 55–80.

Charru, F., E. Larrieu, J.-B. Dupont, and R. Zenit (2007), Motion of a particle near a rough wall in a viscous shear flow, *J. Fluid Mech.*, *570*, 431–453.

Crave, A., and P. Davy (2001), A stochastic "precipiton" model for simulating erosion/sedimentation dynamics, *Comput. Geosci.*, *27*(7), 815–827.

Devauchelle, O., L. Malverti, E. Lajeunesse, C. Josserand, P. Lagree, and K. N. Thu-Lam (2010a), Stability of bedforms in laminar flows with free-surface: From bars to ripples, *J. Fluid Mech.*, *642*, 329–348.

Devauchelle, O., L. Malverti, E. Lajeunesse, C. Josserand, P. Lagrée, and F. Métivier (2010b), Rhomboid beach pattern: A laboratory investigation, *J. Geophys. Res.*, *115*, F02017, doi:10.1029/2009JF001471.

Dietrich, W., and J. Smith (1984), Bed load transport in a river meander, *Water Resour. Res.*, *20*(10), 1355–1380.

Duboys, S. (1879), Le rhone et les rivieres à lit affoillable, *Ann. Ponts Chaussees, Ser.*, *5*, *18*, 141–195.

Einstein, H. (1950), The bed-load function for sediment transportation in open channel flows, *Tech. Bull. 1026*, U.S. Dep. of Agric., Washington, D. C.

Engelund, F., and J. Fredsoe (1976), A sediment transpot model for straight alluvial channels, *Nord. Hydrol.*, *7*(5), 293–306.

Fernandez-Luque, R., and R. Van Beek (1976), Erosion and transport of bed-load sediment, *J. Hydraul. Res.*, *14*, 127–144.

Francis, J. (1973), Experiments on the motion of solitary grains along the bed of a water-stream, *Proc. R. Soc. London, Ser. A*, *332*, 443–471.

Ganti, V., M. Meerschaert, E. Foufoula-Georgiou, E. Viparelli, and G. Parker (2010), Normal and anomalous diffusion of gravel tracer particles in rivers, *J. Geophys. Res.*, *115*, F00A12, doi:10.1029/2008JF001222.

García, M. (2006), ASCE Manual of Practice 110—Sedimentation Engineering: Processes, Measurements, Modeling, and Practice, in *Examining the Confluence of Environmental and Water Concerns: Proceedings of the World Environmental and Water Resource Congress 2006*, edited by R. Graham, p. 94, doi:10.1061/40856(200)94, Am. Soc. of Civ. Eng., Reston, Va.

Gomez, B. (1991), Bedload transport, *Earth Sci. Rev.*, *31*(2), 89–132.

Graf, W., and M. Altinakar (1996), *Hydraulique Fluviale: Écoulement non Permanent et Phénomènes de Transport*, Eyrolles, Paris.

Hjülstrom, F. (1935), Studies of the morphological activity of rivers as illustrated by the River Fyris, *Bull. Geol. Inst. Univ. Uppsala*, *25*, 221–527.

Hu, C. (1996), Bed-load transport. I: Mechnical chararcteristics, *J. Hydraul. Eng.*, *122*, 245–254.

Lajeunesse, E., et al. (2010), Fluvial and submarine morphodynamics of laminar and near-laminar flows: A synthesis, *Sedimentology*, *57*, 1–26.

Lamb, M., W. Dietrich, and J. Venditti (2008), Is the critical shields stress for incipient sediment motion dependent on channel-bed slope?, *J. Geophys. Res.*, *113*, F02008, doi:10.1029/2007JF000831.

Lee, H., and I. Hsu (1994), Investigation saltating particle motions, *J. Hydraul. Eng.*, *120*, 831–845.

Liu, Y., F. Metivier, E. Lajeunesse, P. Lancien, C. Narteau, and P. Meunier (2008), Measuring bed load in gravel bed mountain rivers: Averaging methods and sampling strategies, *Geodin. Acta*, *21*, 81–92.

Métivier, F., P. Meunier, M. Moreira, A. Crave, C. Chaduteau, B. Ye, and G. Liu (2004), Transport dynamics and morphology of a high mountain stream during the peak flow season: The Ürümqi River (Chinese Tian Shan), in *River Flow 2004*, vol. 1, pp. 770–777, A. A. Balkema, Leiden, Netherlands.

Meunier, P., F. Metivier, E. Lajeunesse, A. S. Meriaux, and J. Faure (2006), Flow pattern and sediment transport in a braided river: The "torrent de St Pierre" (French Alps), *J. Hydrol.*, *330*, 496–505.

Meyer-Peter, E., and R. Müller (1948), Formulas for bed-load transport, paper presented at 2nd Meeting of International Association for Hydraulic Research, Int. Assoc. for Hydraul. Res., Stockholm.

Nino, Y., and M. Garcia (1994), Gravel saltation: 1. Experiments, *Water Resour. Res.*, *30*, 1907–1914.

Recking, A., P. Frey, A. Paquier, and P. Belleudy (2009), An experimental investigation of mechanisms involved in bed load sheet production and migration, *J. Geophys. Res.*, *114*, F03010, doi:10.1029/2008JF000990.

Sauermann, G., K. Kroy, and H. Herrmann (2001), Continuum saltation model for sand dunes, *Phys. Rev. E.*, *64*, 31,305–31,305.

Sekine, M., and H. Kikkawa (1992), Mechanics of saltating grains. II, *J. Hydraul. Eng.*, *118*, 536–558.

Shields, I. (1936), Anwendung der ahnlichkeitmechanik und der turbulenzforschung auf die gescheibebewegung, *Mitt. Preuss Vers. Wasserbau Schiffbau*, *26*, 5–24.

Summerfield, M., and N. Hulton (1994), Natural controls of fluvial denudation rates in major world drainage basins, *J. Geophys. Res.*, *99*, 13,871–13,883.

Van Rijn, L. (1984), Sediment transport, part i: bed load transport, *J. Hydraul. Eng.*, *110*, 1431–1456.

Wiberg, P., and J. Smith (1987), Calculations of the critical shear stress for motion of uniform and heterogeneous sediments, *Water Resour. Res.*, *23*, 1471–1480.

Wiberg, P., and J. D. Smith (1989), Model for calculating bed load transport of sediment, *J. Hydraul. Eng.*, *115*, 101–123.

Wong, M. (2003), Does the bedload equation of Meyer-Peter and Müller fit its own data?, paper presented at 30th Congress of the International Association for Hydraulic Research, Int. Assoc. of Hydraul. Res., Thessaloniki, Greece.

Yalin, M. (1977), *Mechanics of Sediment Transport*, Pergamon, New York.

Yalin, M., and A. Ferreira da Silva (2001), *Fluvial Processes*, Int. Assoc. of Hydraul. Eng. and Res., Delft, Netherlands.

F. Charru, Institut de Mécanique des Fluides de Toulouse, CNRS/ Université de Toulouse, 1 Allée du Professeur Camille Soula, F-31400 Toulouse, France.

E. Lajeunesse and L. Malverti, Laboratoire de Dynamique des Fluides Geologiques, Institut de Physique du Globe de Paris, 4 Place Jussieu, F-75252 Paris CEDEX 05, France. (lajeunes@ipgp.jussieu.fr; malverti@ ipgp.jussieu.fr)